STM JOURNALS

Journal of
Polymer & Composites

ISSN: 2321-2810 (Online)
ISSN: 2321-8525 (Print)
Volume 13, Special Issue 1, 2025
DOI (Journal): 10.37591/JoPC

https://journals.stmjournals.com/jopc

Research JoPC

Performance Analysis of Dual Junction Solar Cell Devices utilizing Subcells of $In_{0.51}Ga_{0.49}P$ and GaAs to Study Key Solar Cell Parameters via TCAD based Simulation

Indranil Maity[1,*], Arighna Bhattacharjee[2], Arijit Mondal[2]

Abstract

In the present work, a multi-junction solar cell was designed to obtain better performance over single-junction solar cells. The proposed structure is composed of different layers of diverse semiconductor materials stacked on each other. Here, an $In_{0.51}Ga_{0.49}P$/GaAs double-junction solar cell was outlined as having a distinctive composite material (GaAs) as the tunneling junction. To optimize the solar cell's effectiveness, $In_{0.47}Ga_{0.15}Al_{0.37}P$ was used in the window layer and the back-surface field (BSF) layers. All the optimizations and computations were performed utilizing the Silvaco TCAD software (version: 5.26.1.R), under 1 sun (1370 W/m^2). The light beam of the standard AM1.5G was fired at the solar cell at 300 K, room temperature. With the help of two subcells of the dual-junction solar cell, and by fine-tuning the layer parameters (viz. materials property and material thickness), notable operational parameters were accomplished for the modelled dual-junction solar cells. Our examination centered on the photogeneration rate, energy band diagrams, and the I-V characteristics of the proposed structure in standard test conditions (STC). By connecting the top subcell and the bottom subcell with the intermediate tunnel junction of Gallium Arsenide (GaAs), and by utilizing $In_{0.47}Ga_{0.15}Al_{0.37}P$ for both the BSF and window layers, an efficiency of 25.65% was achieved. The results of the solar cell show an open-circuit voltage (V_{oc}) of 1.74 V, current density at short-circuit condition (J_{sc}) of 16.71 mA/cm^2 and a fill factor (FF) of 88.05%. All the considered layers were lattice-matched, guaranteeing compatibility with the current manufacturing innovations. This study illustrates that through key layer optimizations and progressed re-enactment methods, high-efficiency dual-junction solar cells can be created for their viable usage towards photovoltaic applications in the field of solar energy.

***Author for Correspondence**
Indranil Maity
Email: indrasanu026@gmail.com

[1]Assistant Professor, Department of Electronics and Communication Engineering (ECE), Institute of Engineering and Management (IEM), University of Engineering & Management (UEM), Kolkata, West Bengal, India
[2]Student, Department of Electronics and Communication Engineering (ECE), Institute of Engineering and Management (IEM), Kolkata, West Bengal, India

Received Date: August 12, 2024
Accepted Date: October 24, 2024
Published Date: November 20, 2024

Citation: Indranil Maity, Arighna Bhattacharjee, Arijit Mondal. Performance Analysis of Dual Junction Solar Cell Devices utilizing Subcells of $In_{0.51}Ga_{0.49}P$ and GaAs to Study Key Solar Cell Parameters via TCAD based Simulation. Journal of Polymer & Composites. 2025; 13(Special Issue 1): S829–S837p.

Keywords: Dual-junction solar cells, $In_{0.51}Ga_{0.49}P$ composite material, TCAD modelling, Hybrid compound, Photovoltaic efficiency.

INTRODUCTION

In recent times, solar cells have become crucial in the renewable energy field, offering a clean alternative to fossil fuels. These devices change light energy into electrical energy using the photovoltaic effect. Thus, many major innovations have been made in the structure of solar cells from last decade. One such classification leads to single and multi-junction solar cells based on the number of subcells in the device. Single-junction solar cells (mainly of Silicon) have dominated the market due to their simple design, low production costs, and

established manufacturing processes [1-2]. Silicon forms a single p-n junction, converting sunlight into electricity efficiently, with commercial efficiencies ranging from 15% to 22% [2-3].

On the other hand, multi-junction solar cells are built by stacking many layers of various semiconductor materials, each engineered to absorb specific wavelengths of sunlight. This allows them to capture a larger range of wavelengths of photons compared to simple single-junction cells. The method of stacking materials with different bandgaps in multi-junction solar cells are efficient in trapping photons and thus achieve efficiencies of over 40% under concentrated sunlight [3]. This makes them ideal for high-energy applications like solar power plants and space-based solar arrays. Our work was greatly motivated by the need to enhance the effectiveness and efficiency of dual-junction solar cells beyond conventional limits.

Recent studies have shown major improvements in the performance of dual-junction solar cells through optimized composite material selection, and structural design. For instance, Salem et al. [2] optimized the InGaP/GaAs dual-junction solar cell using the tool Silvaco TCAD, while Bagheri et al. [3] designed a highly efficient dual junction solar cell with a tunnel junction of AlGaAs. Building on this foundation, our research proposes a novel design with an efficiency of 25.65%, and a fill factor of 88.05%, demonstrating a substantial advancement in solar cell technology [4].

By carefully selecting the composite materials, engineering the semiconductor layers and optimizing their electronic and resistive properties, our proposed model aims to capture a larger amount of photons from the sunlight [5] and convert it into electrical energy more effectively. This improvement positions our design as a competitive and efficient solution for renewable energy applications. Thus, looking into the scope of works related to dual-junction solar cells, we aimed to delve deeper into the composite material architecture and junction engineering of these devices. The bottom subcell of the multi-junction solar cell was modelled using gallium arsenide (GaAs) due to its advantageous properties, including a direct bandgap of 1.42 eV that ensures high absorption efficiency, and suitability for thin-film applications (1–5 μm). GaAs is usually well-suited for high-performance environments, offering lower temperature coefficients, and excellent radiation resistance. Though, silicon (Si) is also used in the device modelling of single-junction solar cells as well as primitive cells, but it is less efficient and possesses indirect bandgap, which is less suitable for high efficiency applications. However, other materials can be chosen into the structure, but in this work, they have not been considered due to their suboptimal bandgaps, lower efficiencies, and instability. Therefore, GaAs was precisely selected here for its superior characteristics compared to the other alternatives.

Our research focused on optimizing these aspects to achieve higher efficiency and better performance metrics [6]. The novelty of our work lies in utilizing $In_{0.47}Ga_{0.15}Al_{0.37}P$ as a composite material for the window layer, as depicted in Figure 1(a). This innovative approach provided several advantages. Firstly, the unique composition of the composite material $In_{0.47}Ga_{0.15}Al_{0.37}P$ improved the optical properties of the window layer, enhancing the illumination and absorption of incident light. This resulted in a more efficient photogeneration process, where a higher number of electron-hole pairs were generated. Additionally, the improved material properties led to better carrier mobility and reduced recombination losses, which are critical for achieving higher efficiency in solar cells. This novel material used in this approach can open new avenues for high-performance applications, particularly in batteries and energy composites.

STRUCTURAL MODELING AND SIMULATIONS:

Designed Structure

The Dual-Junction solar cell was modelled using several semiconductor layers, where each layer absorbs specific parts of the solar spectrum. Each layer along with its dimensions, doping concentration, and materials are listed in Table 1. The topmost layer, the window made of InAlGaP, is transparent and minimizes reflection to allow maximum light to reach the active layers. InAlGaP has the material

properties of refractive index of 3.49, absorption coefficient of 50536 cm^{-1} and a direct bandgap energy of 1.7-3.1 eV, which makes it a suitable composite material for the window layer. InAlGaP is commonly synthesized via hetero-epitaxy on gallium arsenide or gallium phosphide substrates. A certain composition of InAlGaP thus was chosen so that the bandgap matches the energy of a particular visible light wavelength. The top sub cell, made of wide bandgap material InGaP was used to absorb the highly energized photons from the blue end of the solar spectrum, while lower energized photons pass to the next layers [7]. The Back Surface Field (BSF) layer of GaAs, with a narrower bandgap, enhanced minority carrier collection by creating an electric field that reduces recombination losses. Gallium arsenide (GaAs) is a compound semiconductor with a direct bandgap of 1.42 eV [8]. It also has superior electron mobility (9000 cm^2/v.s at 300 K) compared to silicon, enabling high-speed electronic applications. The tunnel junction, composed of heavily doped GaAs layers, acts as a low resistance series connection among the two sub cells. The bottom sub cell, typically GaAs, had the smallest bandgap and absorbed the low energy photons present in the red and infrared regions. Front and back metallic contacts extracted the generated electrical current [9-10].

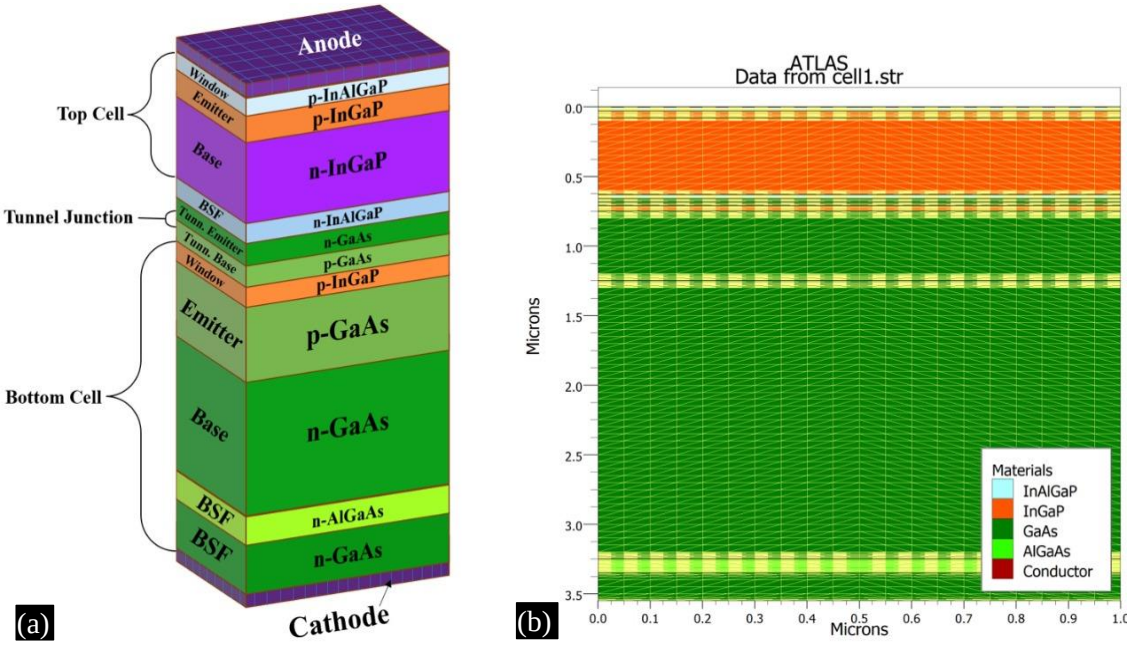

Figure 1. (a) 3D Representation of the Proposed Dual-Junction Solar Cell, and (b) Meshing Profile of the Proposed Structure

Table 1. Device Design Parameters and Layer-Wise Structure for the Proposed Dual-Junction Solar Cell.

Region	Composite Material	Dimension (µm)	Doping concentration
Window	InAlGaP	0.030	2e18 (p-type)
Emitter	InGaP	0.050	2e18 (p-type)
Base	InGaP	0.550	7e16 (n-type)
BSF	InAlGaP	0.030	2e18 (n-type)
Tunnel emitter	GaAs	0.015	5e19 (n-type)
Tunnel base	GaAs	0.025	3e19 (p-type)
Window	InGaP	0.040	3e18 (p-type)
Emitter	GaAs	0.500	2e18 (p-type)
Base	GaAs	2.000	7e16 (n-type)
BSF	AlGaAs	0.100	5e18 (n-type)
BSF	GaAs	0.200	1e18 (n-type)

Simulation Methods

The simulation of electronic properties [11] for the proposed model was conducted using Silvaco TCAD (*version: 5.26.1.R*), a robust tool for semiconductor device simulation [12]. During device modelling, we introduced denser meshing between the junctions for better convergence in calculations, as shown in Figure 1(b). The following models were employed to calculate electronic properties:

models temperature =300 fermi optr print bgn.

The temperature was set to 300K [13], representing standard testing conditions (STC), while the Fermi level and bandgap narrowing (bgn) effects were considered. These modelling methodologies are crucial for accurately predicting the behaviour of charge carriers under thermal equilibrium. The output parameters included many simulation methods i.e. commands in the Silvaco TCAD due to these outputs provide detailed insights into various physical properties such as optical intensity, band structure temperatures, conduction and valence band edges, charge distributions, polarization charges, band parameters, and carrier mobilities. Specifically, *e.mobility,* and *h.mobility* refer to electron and hole mobilities, respectively, which are critical for understanding carrier transport mechanisms. The terms *u.srh, u.radiative,* and *u.auger* denote the different recombination rates, each of which plays a significant role in carrier lifetime and recombination losses.

An AM1.5G solar spectrum was used to simulate light absorption. The setup placed the origin of the light beam at coordinates (0.5, -2) with a perpendicular incidence angle of 90 degrees. The AM1.5G spectrum is a standard reference for terrestrial solar cell testing, representing the solar irradiance at the level of Earth's surface with an air mass of 1.5 [14]. The syntax for modelling the composite materials with user-defined compositions is given as follows in Table 2.

Table 2. ATLAS Syntax for Defining Relative Compositions of Hybrid Compounds.

Composite Material	Syntax
InGaP	$In_{(1-x)}\ Ga_{(x)}\ P$
InAlGaP	$In_{(1-x-y)}\ Al_{(x)}\ Ga_{(y)}\ P$

RESULTS AND DISCUSSION:

Photogeneration Rate

The photogeneration rate gradually deteriorated through the layers, reflecting effective photon absorption. A sharp drop was observed at the InAlGaP and AlGaAs BSF layers due to their metallic properties. Figure 2(a-b) reveals that the highest photogeneration rate occurred near the surface layer of InAlGaP, indicating strong absorption [15], and efficient photogeneration. This drop was caused by several factors: the high bandgap of BSF layers, which made them less efficient at absorbing photons, and the BSF's primary role of creating a potential barrier to reflect minority carriers into the active region, reducing recombination losses. Additionally, light absorption was intended mainly for the top and middle cells, optimized for high photogeneration [16]. By the time light reached the BSF layer, most usable photons had already been absorbed. Efforts focused on optimizing the BSF layer's thickness and doping concentration to balance its electrical and optical properties. This drop is a common characteristic in multi-junction solar cells, accepted as a trade-off for improved overall efficiency.

Energy Band Diagram

The energy band illustration (Figure 3) of our designed solar cell revealed several key features. In the top cell region, the conduction and valence bands were well-separated, promoting efficient electron-hole pair generation. The tunnel junction showed sharp band alignments, enabling effective carrier transport between the cells. In the bottom cell region, the bands maintained their separation, ensuring continued charge generation [17]. The distinctive energy dips and rises at specific positions indicated the presence of optimized window and BSF layers, contributing to reduced recombination losses and enhanced carrier collection.

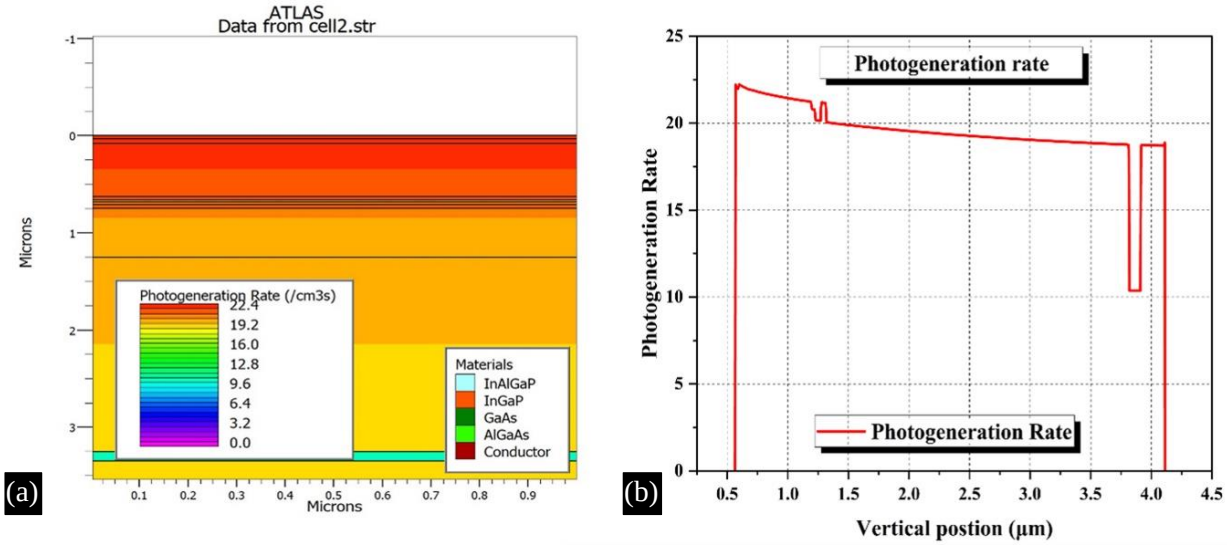

Figure 2. (a) Contour of the Photogeneration Rate across the Designed Structure, and (b) Variation in the Photogeneration Rate.

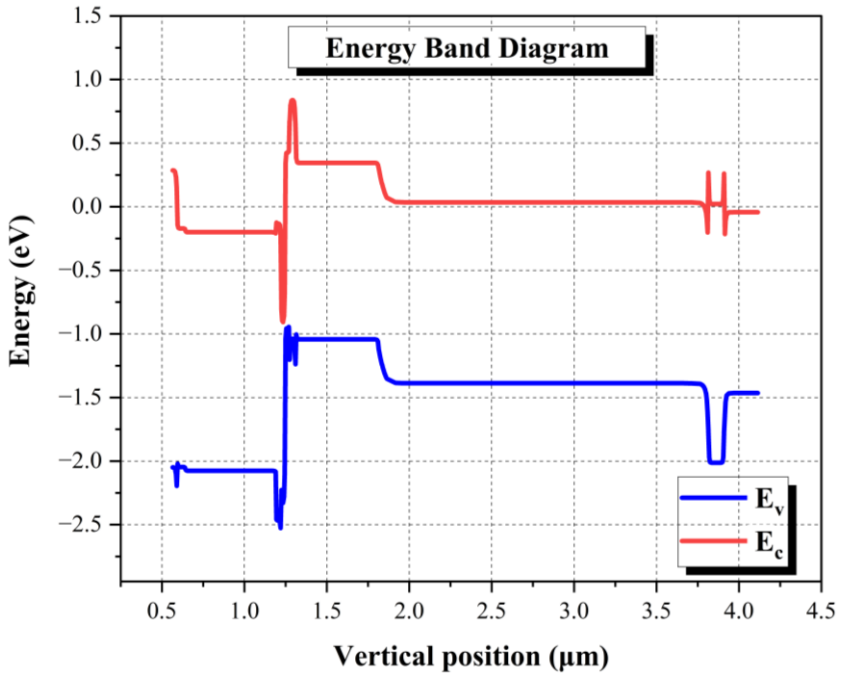

Figure 3. The Energy Bandgap Profile of the Proposed Structure along it's Vertical Cross-Section.

Current-Voltage Behaviour

The current-voltage behaviour of the solar cell structure were meticulously analysed based on the provided graph as depicted in Figure 4(a-b), and the detailed composition of the materials used. The dark current, represented by the black line, remained nearly constant, and close to zero across the voltage range from 0 V to 2 V. This minimal current flow in the absence of light is indicative of negligible thermally generated charge carriers, underscoring the high-quality material and the effective suppression of dark current. Conversely, the light current, depicted by the red line, exhibited a significant increment compared to dark current till 1.7 V, followed by a sharp decline. The internal electric field generated at the p-n junctions, facilitates the separation of these carriers, resulting in a significant photocurrent. The rise in light current up to 1.7 V, followed by a decline, is indicative of avalanche breakdown. This event is caused by the high electric field built in the depletion region which

in turn causes ionization, leading to a sudden surge in current followed by saturation as the carriers are rapidly generated and swept across the junction [18]. The I-V characteristics observed in this study underscored the efficacy of the dual-junction cell design in optimizing photon absorption and carrier generation. The sharp breakdown observed in the light current highlights the material's response to high electric fields, and provides valuable insights into the operational limits and efficiency of the cell under varying illumination conditions.

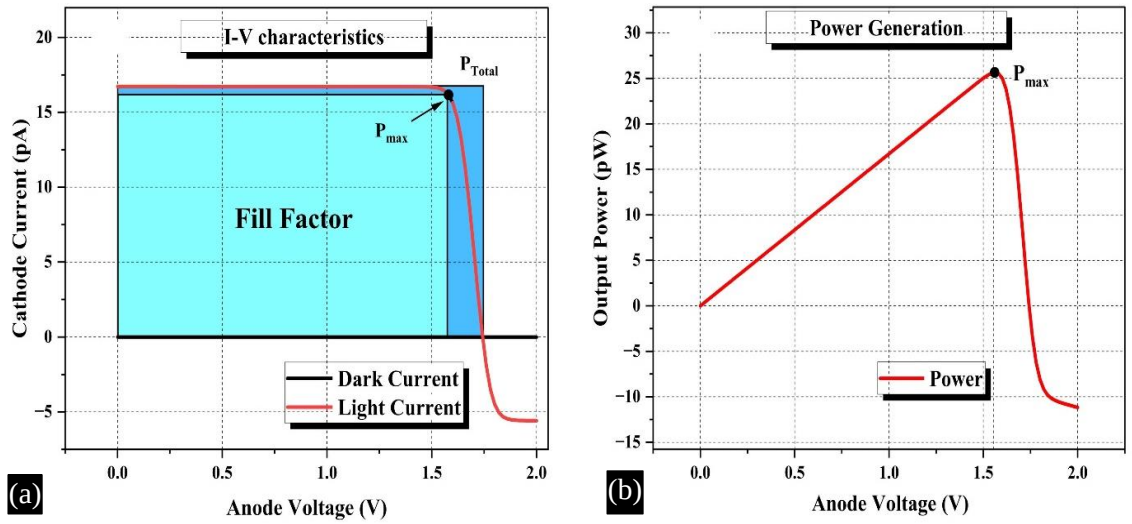

Figure 4. (a) The I-V Characteristics along with the Fill Factor Representation, and (b) Power Generation Graph

Fill Factor (FF)

The fill factor measures how ideal the I-V curve is, which is visually represented by the shaded sky-blue region relative to the total possible area. A higher fill factor indicates a more efficient solar cell, operating closer to its maximum power output over a larger portion of its I-V curve. The total power (P_{total}) is represented by the entire blue rectangle area (as shown in Figure 4(a)), formed by the open-circuit voltage (V_{oc}) and short-circuit current (I_{sc}). Our proposed model provides a fill factor (FF) of 88.05%, which further signifies the quality of the proposed structure of solar cell.

Efficiency (η)

The solar cell model demonstrated a remarkable output efficiency (η) of 25.65%, indicating its proficiency in converting incident solar radiation into electrical energy [19]. The high fill factor indicates that the cell experiences minimal resistive losses, both in terms of series resistance (which affects the flow of current), and shunt resistance (which affects the leakage current paths within the cell). This balance is essential for achieving high efficiency. The V_{oc} of 1.74V is largely determined by the bandgap energies of the different materials, used in the layers of this solar cell model. The voltage was generated by the separation of photogenerated electron-hole pairs at the junctions. Higher bandgap materials typically result in higher V_{oc} because they can withstand higher electric fields without breaking down [20-21]. The J_{sc} of 16.71 mA/cm² reflects the cell's ability to generate a high density of charge carriers under illumination. High quantum efficiency implies effective light absorption and minimal recombination losses [22].

The efficiency of our proposed structure (η) can be expressed by (Eq. 1):

$$\eta = \frac{P_{max}}{P_{in}} = \frac{V_{OC} \times J_{SC} \times FF}{P_{in}} \quad (1)$$

where, P_{max} is the maximum output power, and P_{in} is the incident power. All the quantitative results observed by our proposed dual-junction solar cell are listed in Table 3.

Table 3. Quantitative Results (Key Parameters) Observed from the Designed Solar Cell.

V_{oc}	J_{sc}	FF	Efficiency	P_{max}
1.74 V	16.71 mA/cm²	88.05%	25.65%	25.54 pico-watt

Effect of Temperature Variation

The performance of dual-junction solar cells is considerably affected by temperature variations, which are a critical factor in solar energy applications. In the graph provided in Figure 5, the output characteristics of the proposed solar cell model were simulated under different temperature conditions, specifically at 293 K, 300 K (27°C), 310 K, 325 K, and 350 K. The atmospheric temperature, 300 K (27°C), is considered a reference point for comparing the cell's behaviour under other four temperature conditions.

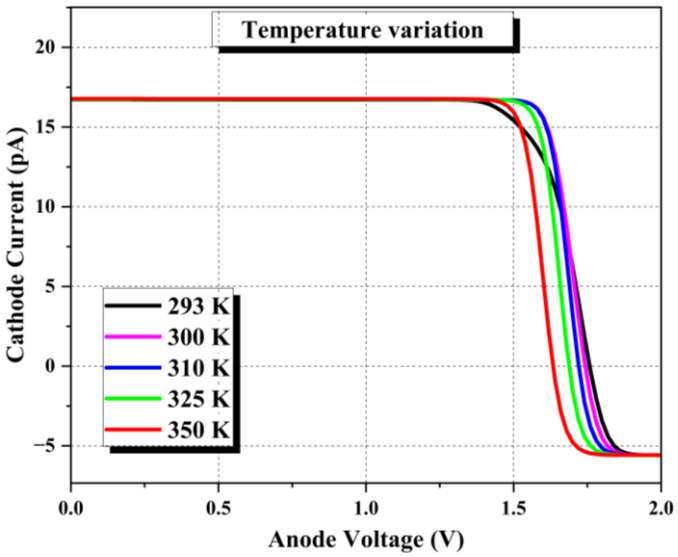

Figure 5. Variation of I-V Characteristics at Different Operational Temperatures.

As the temperature increased, band bending occurred in the semiconductor materials used in the solar cell, such as InGaP, GaAs, and InAlGaP. This bending led to a reduction in the V_{oc} of the cell. The graphs clearly showed this effect, where at 350 K, the voltage at which the current started to drop was noticeably lower compared to 293 K (with 300 K as the reference point). This was a direct result of the decreased bandgap energy at higher temperatures, which lowered the voltage. Moreover, higher temperatures led to an increase in carrier recombination within the cell. This meant that more electron-hole pairs recombined before they could generate photocurrent, thus reducing the cell's overall output efficiency.

The relationship between temperature and open-circuit voltage (V_{oc}) can be further theoretically quantified using the equation $\frac{\partial V_{oc}}{\partial T} = \frac{V_{oc}}{T} + \frac{nkT}{q}\left(\frac{1}{J_{SC}}\frac{\partial J_s}{\partial T} - \frac{1}{J_0}\frac{\partial J_0}{\partial T}\right)$, as reported by Maka et al. [23], where J_{sc} denotes short-circuit current density of the solar cell and J_o represents reverse saturation current density. Moreover, the V_{oc} of the solar cell increases with an increment of illumination, and decreases with an increment of temperature. Consequently, the efficiency of our proposed model design, which is depended on both V_{oc} and FF, deteriorated as the temperature rose.

CONCLUSION

In this study, a dual-junction solar cell comprising $In_{0.51}Ga_{0.49}P$/GaAs with GaAs as the tunnelling junction was meticulously designed and simulated using Silvaco TCAD. The introduction of $In_{0.47}Ga_{0.15}Al_{0.37}P$ as a composite material for the window and the back-surface field (BSF) layers

marked a significant improvement in the cell's efficiency. This material configuration enabled the solar cell to achieve a power conversion efficiency of 25.65%. The photogeneration rate analysis indicated strong absorption and effective photogeneration at the surface layer of InAlGaP, with a gradual decline through the layers, reflecting efficient photon absorption. The I-V characteristics showed minimal dark current, highlighting the quality of the materials, and the suppression of thermally generated charge carriers. The results from our study indicated that the proposed $In_{0.51}Ga_{0.49}P$/GaAs dual junction solar cell structure excelled in achieving a higher fill factor (FF) of 88.05%, and V_{oc} of 1.74 V compared to the CIGS-based tandem structures. Our optimized cell structures exhibited higher efficiencies as well as superior fill factor. Extensive use of Silvaco TCAD device modelling has proved to yield better outcomes. The output methodologies used in the simulations were thoroughly studied and thus provides the desired results. The high fill factor was indicative of the efficient charge carrier extraction, and reduced recombination losses in our design, making it a promising candidate for future use in high performance photovoltaic applications and batteries.

REFERENCES

1. Benlekhdim A, Cheknane A, Sfaxi L, Hilal HS. Efficiency improvement of single-junction InGaP solar cells by advanced photovoltaic device modeling. *Optik*. 2018 Jun 1;163:8–15.
2. Salem MS, Saif OM, Shaker A, Abouelatta M, Alzahrani AJ, Alanazi A, Elsaid MK, Ramadan RA. Performance optimization of the InGaP/GaAs dual-junction solar cell using SILVACO TCAD. *International Journal of Photoenergy*. 2021;2021(1):8842975.
3. Bagheri S, Talebzadeh R, Sardari B, Mehdizadeh F. Design and simulation of a high efficiency InGaP/GaAs multi junction solar cell with AlGaAs tunnel junction. *Optik*. 2019 Dec 1;199:163315.
4. Maity I, Acharyya D, Huang K, Chung P, Ho M, Bhattacharyya P. A comparative study on performance improvement of ZnO nanotubes based alcohol sensor devices by Pd and rGO hybridization. *IEEE Transactions on Electron Devices*. 2018 Jun 29;65(8):3528–34.
5. Chawla R, Singhal P, Garg AK. Design and analysis of multi junction solar photovoltaic cell with graphene as an intermediate layer. *Journal of nanoscience and nanotechnology*. 2020 Jun 1;20(6):3693–702.
6. Kumari M. A comparative study of acoustical phonon induced and optical phonon induced parametric gain in AIIIBV type semiconductor-magneto-plasmas. *RP Materials: Proceedings*. 2022 Aug 24;14:16.
7. Maity I, Bhattacharyya P. Room temperature acetone sensing performance of rGO-ZnO nanotubes binary hybrid structure. *Sensor Letters*. 2019 Jun 1;17(6):417–22.
8. Soley SS, Dwivedi AD. Numerical simulation and performance analysis of InGaP, GaAs, Ge single junction and InGaP/GaAs/Ge triple junction solar cells. *Materials Today: Proceedings*. 2021 Jan 1;39:2050–5.
9. Singh HP. Nonlinear absorption of ternary and quaternary semiconductor nanocrystals. *RP Cur. Tr. Eng. Tech.* 2022; Vol. 1(Part 1):13–6.
10. Suria BS, Hussain SH, Mehmood HA, ALI G. Nanocrystalline silicon (nc-Si: H) and amorphous silicon (a-Si: H) based thin-film multijunction solar cell. *Sains Malaysiana*. 2014;43(6):895–8.
11. Maity I, Nagasawa H, Tsuru T, Bhattacharyya P. Correlation between ammonia selectivity and temperature dependent functional group tuning of GO. *IEEE Transactions on Nanotechnology*. 2020 Dec 18;20:129–136.
12. Kowsar A, Billah M, Dey S, Debnath SC, Yeakin S, Farhad SF. Comparative study on solar cell simulators, *2nd International Conference on Innovation in Engineering and Technology (ICIET)* 2019 Dec 23; 1–6.
13. Hu Y, Chen B, Xu P. A comprehensive simulation study of multi-junction solar cell. *Materials Research Express*. 2024 May 9;11(5):056201.
14. Benaicha M, Dehimi L, Pezzimenti F, Bouzid F. Simulation analysis of a high efficiency GaInP/Si multijunction solar cell. *Journal of Semiconductors*. 2020 Mar 1;41(3):032701.
15. Maity I, Ghosh K, Rahaman H, Bhattacharyya P. Tuning of electronic properties of edge oxidized armchair graphene nanoribbon by the variation of oxygen amounts and positions. *Journal of Materials Science: Materials in Electronics*. 2017 Jun;28:9039–47.

16. Nayak PP, Dutta JP, Mishra GP. Efficient InGaP/GaAs DJ solar cell with double back surface field layer. *Engineering Science and Technology, an International Journal*. 2015 Sep 1;18(3):325–35.
17. Singh J. Simplified model to derive the statistics of photon propagation through an optical coupler and an optical fibre. *RP Materials: Proceedings*. 2022; Vol. 1, (Part 1); 17–21.
18. Maity I. Cadence Virtuoso based circuit simulation of universal logic gates: A board tutorial. *RP Cur. Tr. Eng. Tech.* 3. 2024; Vol. 3 (No. 1); 1–7.
19. Djaafar F, Hadri B, Bachir G. Optimal parameters for performant heterojunction InGaP/GaAs solar cell. *International Journal of Hydrogen Energy*. 2017 Mar 30;42(13):8644–9.
20. Maity I, Ghosh K, Rahaman H, Bhattacharyya P. Selectivity tuning of graphene oxide based reliable gas sensor devices by tailoring the oxygen functional groups: A DFT study based approach. *IEEE Transactions on Device and Materials Reliability*. 2017 Oct 25;17(4):738–45.
21. Laoufi, A. M., Dennai, B., Kadi, O., & Fillali, M. Numerical modeling of multi-junction solar cell-based CIGS with two sub-cells in parallel using Silvaco TCAD. *Chalcogenide Letters*. 2021;18(6), 297–301.
22. Boukortt NE, Patanè S, AlAmri AM, AlAjmi D, Bulayyan K, AlMutairi N. Numerical investigation of perovskite and u-CIGS based tandem solar cells using silvaco TCAD simulation. *Silicon*. 2023 Jan;15(1):293–303.
23. Maka AO, O'Donovan TS. Effect of thermal load on performance parameters of solar concentrating photovoltaic: High-efficiency solar cells. *Energy and Built Environment*. 2022 Apr 1;3(2):201–9.

